

## SUPPORTING INFORMATION

# Single Molecule Nonlinearity in a Plasmonic Waveguide

Christian Schörner<sup>†</sup> and Markus Lippitz<sup>†,\*</sup>

<sup>†</sup> Experimental Physics III, University of Bayreuth, Universitätsstr. 30, 95440 Bayreuth, Germany

Corresponding Author

\* Email: markus.lippitz@uni-bayreuth.de

### **table of content**

Figure S1: Sample fabrication

Figure S2: Optical setup

Figure S3: Pump and depletion spot size

Figure S4: Depletion statistics of TDI

Figure S5: Lifetime histogram of TDI

Figure S6: Quantifying the background emission

Figure S7: Propagation of the depletion pulses

Figure S8: Propagation loss with PMMA cover

Supplementary note 1: numerical simulations

Supplementary note 2: model for fluorescence suppression

## SAMPLE FABRICATION

---

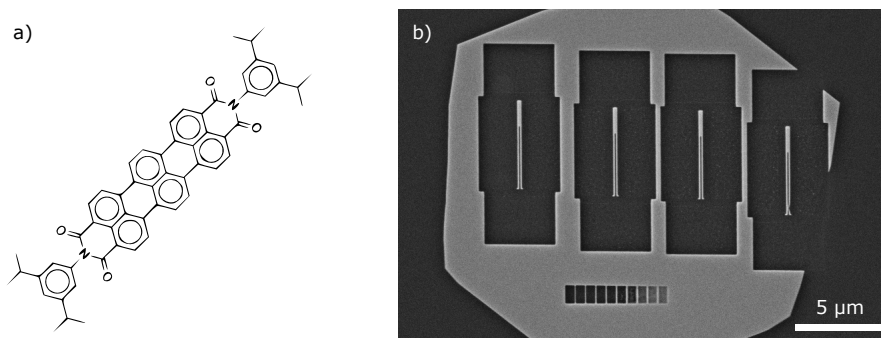


Figure S1: (a) Terrylene diimide was bought from KU dyes ApS, Copenhagen. As matrix material we use a PMMA resist (ARP671.015, Allresist) that was further diluted to 0.5% solid content. The solution was doped with TDI at a very low  $< 10^{-9}$  mol/L concentration and spin coated on the waveguide sample at 1000 rotations per minute resulting in a film thickness of only about 10 nm. For ensemble measurements, a higher concentration of TDI was used. (b) The waveguide fabrication is performed by focused ion beam milling (Scios, FEI company) using Ga ions at 30 kV acceleration voltage and 49 pA ion current. The waveguide circuits are milled in a thin silver flake (height 80 nm) on glass covered with a thin conductive layer (Electra 92, Allresist). The conductive layer is easily removed after milling via DI water. As a result, silver waveguides are remaining, well separated ( $>2 \mu\text{m}$ ) from the silver flake for optical measurements. Furthermore, the silver nanostructures are encapsulated with a thin layer of  $\text{Al}_2\text{O}_3$  deposited by atomic layer deposition (Savannah, Ultratech). We use 60 cycles of water and TMA precursor-pulses at  $100^\circ\text{C}$  deposition temperature, yielding a layer of about 5 nm in thickness. For the optical measurements in this work the three nanostructures on the left side (same fabrication parameters) have been used. The structure at the right side was excluded due to a fabrication imperfection.

## OPTICAL SETUP

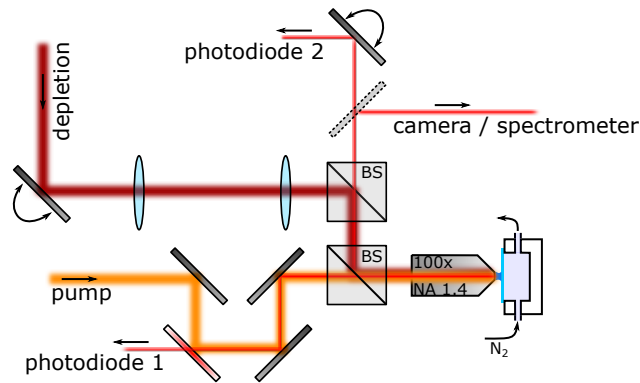


Figure S2: Simplified sketch of the setup. As light source we use a supercontinuum white light laser (SuperK EXTREME EXR-15, NKT Photonics) equipped with a tunable single line filter (SuperK Varia, NKT Photonics). The output spectrum (610-770 nm) is split into a pump and depletion path via a dichroic mirror (zt 635RDC, AHF Analysentechnik). Bandpass filters define the final spectral ranges of the pump (BP 625/30, AHF) and depletion path (2x BP 769/41, AHF). Polarizers (LPVIS100-MP and WP25M UB, Thorlabs) can be inserted to define a linear polarization. The two light paths are superimposed in front of the objective by two 50:50 beamsplitters (BS016 and BS013, Thorlabs). The focus position of the depletion pulses on the sample can be scanned via a piezo mirror platform (S-334.2SL, Physik Instrumente) equipped with a piezo controller (E-501.00, Physik Instrumente), followed by a 4f-system consisting of two lenses (250 mm and 300 mm focal length). The setup offers two detection paths. Light in path 1 passes the 50:50 beamsplitter, a dichroic mirror (HC BS650, AHF) and dielectric longpass (LP635, AHF) and shortpass (SP710, SP730) filters and is finally focused to avalanche photodiode 1 (MPD PDM Series, Picoquant) via a 150 mm tube lens. The light in path 2 is reflected by the first beamsplitter, transmitted by the second beamsplitter and then several detectors can be selected by flip mirrors. First, the light can be guided to an avalanche photodiode 2 (MPD PDM Series, Picoquant) via a scanning mirror (PSH 25, Piezosystem Jena) equipped with a piezo controller (d-Drive, Piezosystem Jena) and a tube lens (150 mm focal length). Second, the light in path 2 can be guided toward the CMOS camera (Zyla 4.2, Andor) with a tube lens of 200 mm. Third, the light in path 2 can be guided to a spectrometer (Isoplan 160 with ProEM EMCCD camera, Princeton Instruments). For fluorescence measurements via path 2 a longpass filter (LP647, AHF) is flipped in the detection path. The fluorescence in case of the two-pulse experiment is detected via the photodiode in path 1. Both photodiodes have a detection spot size with about 600 nm diameter in the sample plane. The pulse energies of the pump pulses have been about 1 pJ. All pulse energies are given in the sample plane after passing the objective. Typically, the integration time was 2 s for the imaging camera and 10 s for the spectrometer camera. The time bin of figure 4b in the main manuscript was 80 ms. In all camera images a mean background has been subtracted.

## PUMP AND DEPLETION SPOT SIZE

---

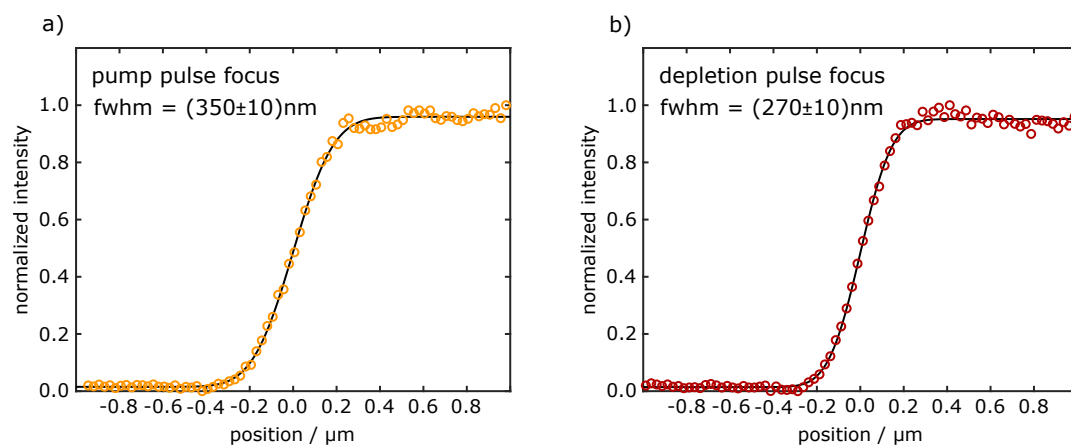


Figure S3: Laser spot sizes measured by scanning the sharp edge of a silver flake across each laser focus and recording the reflected intensity. The experimental data (averaged over 5 consecutive scans) is shown as colored circles while the fit of an error-function is shown as black solid line. The polarization is set parallel to the edge to avoid the excitation of surface plasmons. The full width at half maximum for the pump-pulse (a) and depletion-pulse (b) focus is calculated from the width of the error-function.

## DEPLETION STATISTICS OF TDI

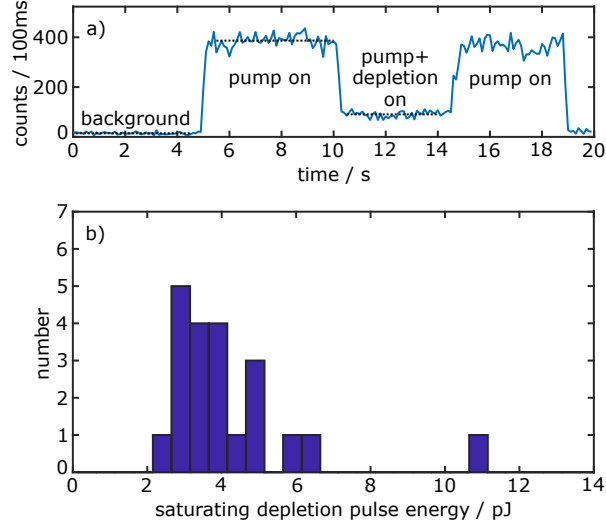


Figure S4: (a) Time trace of the emission of a single TDI molecule in PMMA. The pump is switched on at 5 s and the depletion pulses ( $E_{\text{depletion}} = 3.9 \text{ pJ}$ ) are added during about 10–15 s. At 19 s the pump is turned off. The fluorescence suppression  $\eta$  is calculated using the three relevant intensity levels (black dashed). Subsequently, the saturating depletion pulse energy is calculated according to  $E_{\text{sat}} = -E_{\text{depletion}}/\ln(\eta)$ . The single-step photobleaching event has been checked for all molecules shown here and for the one in figure 2b of the main manuscript. (b) Histogram of the saturation depletion pulse energy for different single TDI molecules. We attribute the variation of the saturation depletion pulse energy from molecule to molecule mainly to the random orientation of the TDI molecules in the PMMA film. These measurements have been performed with unpolarized depletion pulses. Thus, in-plane variations of the molecular orientation do not impact the measurements. By contrast, out-of-plane variations of the orientation lead to a distribution of the saturating depletion energies. As a consequence, a low value in the saturating depletion energy corresponds to an in-plane orientation of the molecule. The smallest saturating depletion pulse energy in the histogram is about 2.4 pJ, corresponding to a molecule with in-plane orientation.

The (antisymmetric) plasmonic mode in our waveguide is excited by perpendicular polarization. Thus, to make a fair comparison for a linear polarization, we divide the lowest number in the histogram by 2. This ends up in the value of 1.2 pJ, which corresponds to a molecule with in-plane orientation well aligned with a linear polarization of the depletion pulses in a Gaussian focus. This number should be used as a reference to compare with the depletion via a single plasmonic mode.

## QUANTIFYING THE BACKGROUND EMISSION

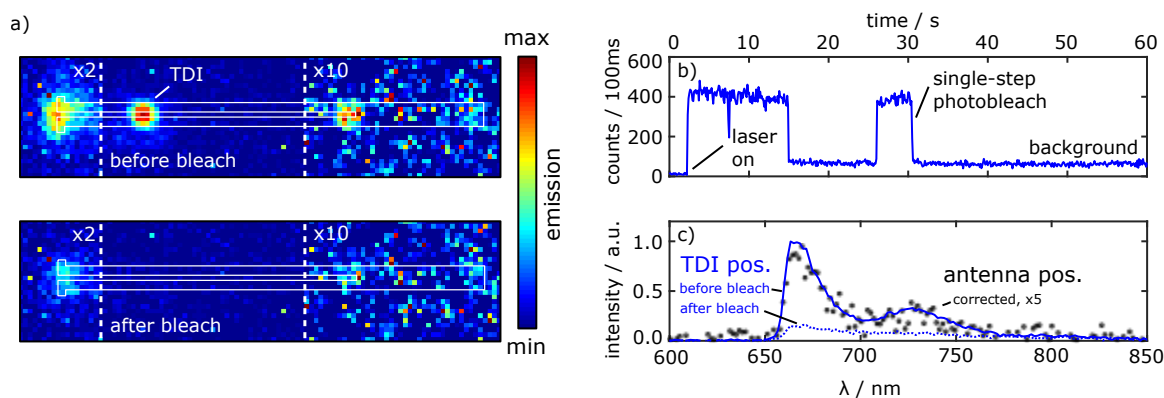


Figure S5: (a) Fluorescence image of the waveguide structure before (top) and after (bottom) photobleaching of the TDI. The pump-pulses are focused on the antenna with perpendicular polarization. After photobleaching, the emission spot along the gap, as well as most emission at the inner end of the mode detector, vanishes. Furthermore, the emission at the excitation position (antenna) is strongly reduced. This demonstrates that all emission spots, including the plasmonic signals at the waveguide ends, stem predominantly from the same molecule in the gap. (b) Time trace of the emission at the TDI position demonstrating a single-step photobleaching of the coupled TDI. (c) Spectrum recorded at the TDI position (blue, solid) before the photobleaching event resembling the emission spectrum of TDI molecules with a vibronic progression. After the photobleaching a weak and unstructured broad spectrum (blue, dotted) is detected at that position. The spectrum at the antenna - corrected by the background emission collected after the photobleaching - is shown as black dots (multiplied by a factor of 5). We attribute the weak background emission, which is present at the excitation position even after photobleaching of the TDI, to luminescence of silver. Other dye molecules are excluded as origin, as the signal is stable, i.e. does not show bleaching, and differs in the emission spectrum.

## LIFETIME HISTOGRAM OF TDI

---

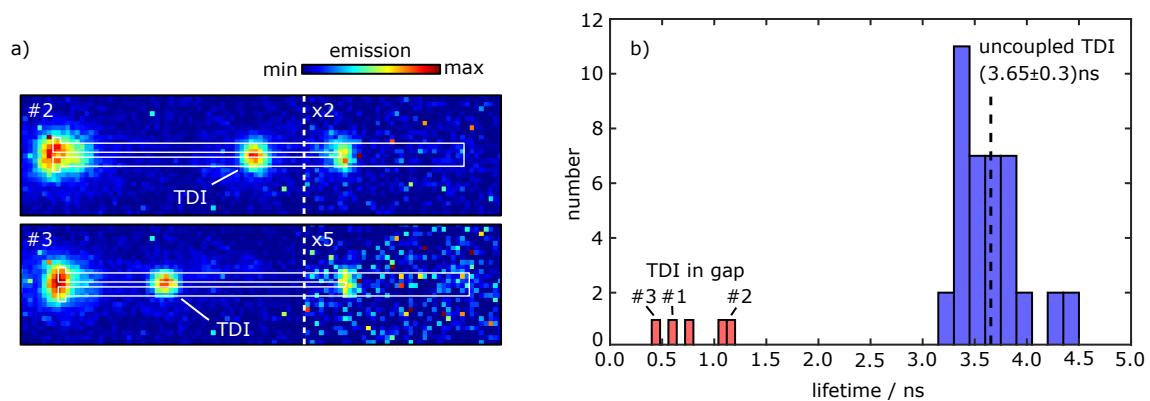


Figure S6: (a) Fluorescence images of additional exemplary datasets #2 and #3 of a single TDI molecule in the gap of the waveguide structure. The fluorescence image of dataset #1 is shown in the main manuscript and Figure S5. The pump pulse focus is positioned on the antenna with perpendicular polarization in all cases, which results in a contribution of silver luminescence at this position (c.f. Figure S5). (b) Lifetime histogram of TDI in the uncoupled case (blue) and in the gap of the waveguide structure (red) detected directly at the TDI position with a detection spot size of 600 nm in diameter.

## PROPAGATION OF THE DEPLETION PULSES

---

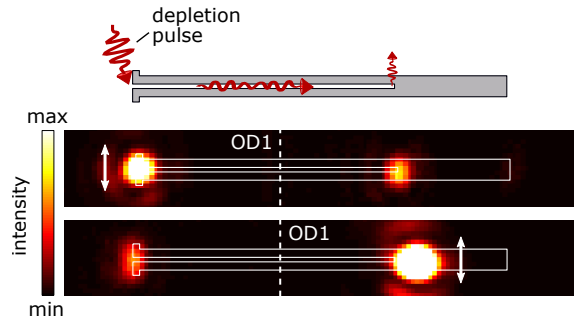


Figure S7: Far-field imaging of the propagation of the depletion pulses via gap-plasmons (antisymmetric mode) upon focusing on the antenna (top) and near end of the mode detector (bottom). Without PMMA cover the transmission is 0.3%, whereas with PMMA cover the transmission reaches 0.12%, likely reduced due to the increased refractive index in the gap. We define the transmission as the power scattered from the waveguide end in the collection angle of the objective relative to the applied power at the excitation spot. The latter we determine from its reflection at a cleaned substrate surface, corrected by the surface reflectivity. In total, this transmission includes the incoupling, propagation, and out-coupling/collection efficiency.

## PROPAGATION LOSS WITH PMMA COVER

---

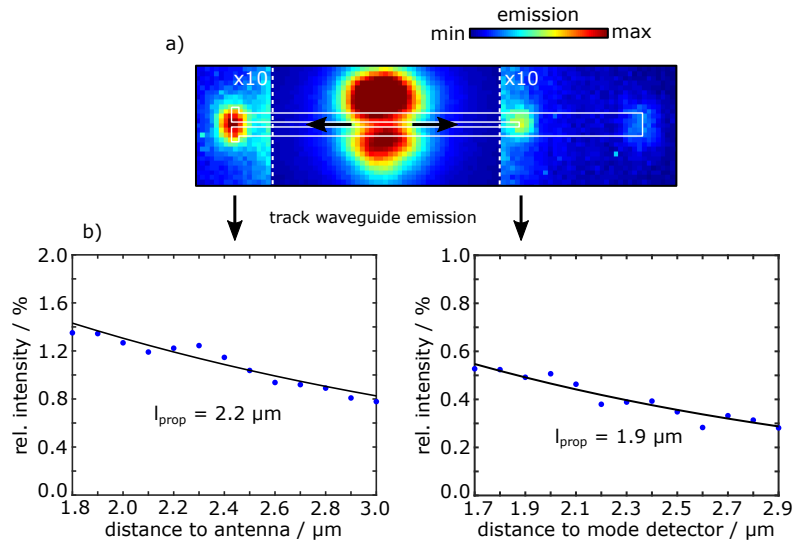


Figure S8: (a) Fluorescence image of an ensemble of TDI molecules in a PMMA layer on the waveguide structure with a pump focus at the center and polarized perpendicular to the long nanowires' axis. (b) The waveguide emission at the antenna (left) and inner end of the mode detector (right) normalized to the emission at the excitation position. The propagation loss is determined by a single exponential fit, yielding a value of about  $2 \mu\text{m}$  with the PMMA cover. Without the PMMA cover the propagation length is expected to be higher as the transmission of the structure is increased by a factor of 2.5 (see Figure S7).

## SUPPLEMENTARY NOTE 1: NUMERICAL SIMULATIONS

---

Electromagnetic near-fields are calculated using the commercial software package Comsol Multiphysics. The refractive index for silver is taken from Johnson and Christy[1]. The air and substrate are modeled by the refractive index 1.0 and 1.5, respectively. The near-to-far-field transformation was computed using a method based on reciprocity arguments using a freely available software package [2]. For imaging, the far-field is first refracted at the objective and tube lens taking the finite numerical aperture of the objective into account. The propagation to the image plane is subsequently performed by a Fourier transform [3]. The far-field imaging simulation is performed with an in-plane dipole ( $\lambda = 680$  nm) oriented across the gap in 20 nm height above the substrate. The thin cover (ALD and PMMA) layer is neglected for numerical simplicity of the full 3-dimensional model.

## SUPPLEMENTARY NOTE 2: MODEL FOR FLUORESCENCE SUPPRESSION

---

The model of the intensity cross-section  $I$  (units: counts per 80 ms time bin) in figure 4c of the main manuscript as function of the position along the waveguide  $x$  is given by:

$$I(x) = I_{bg} + I_{TDI} \sum_n \exp(-a_n G(x - x_n)) \quad . \quad (1)$$

The background level is fixed to  $I_{bg} = 24$  counts, determined by the dark counts of the detector and weak luminescence of the silver.  $I_{TDI}$  represents the average undisturbed TDI fluorescence counts. Normalized Gaussian spots  $G(x)$  at the positions  $x_n$  of antenna, molecule, and mode detector, are taken as input to the exponential suppression.  $a_n$  describes the saturation factor by which the depletion pulse fluence applied to the molecule exceeds the saturating pulse fluence. An optimization of all non-fixed variables is performed, resulting in  $I_{TDI} = 81$  and the suppression factors  $\eta_n = \exp(-a_n)$  given in figure 4c of the main manuscript. The intrinsic width of the Gaussian is about 450 nm, probably broadened compared to the focus size (Figure S3) due to the finite size of the silver nanostructure and finite pixel size. The exponential function further broadens the resulting width of the fluorescence suppression dip. This effect is most pronounced in the saturation regime, c.f. the position of the molecule in figure 4c of the main manuscript.

## BIBLIOGRAPHY

---

- [1] Johnson, P. B. & Christy, R. W. "Optical Constants of the Noble Metals." In: *Phys. Rev. B* 6 (12 1972), pp. 4370–4379.
- [2] Yang, J., Hugonin, J.-P., & Lalanne, P. "Near-to-Far Field Transformations for Radiative and Guided Waves." In: *ACS Photonics* 3.3 (2016), pp. 395–402.
- [3] Novotny, L. & Hecht, B. *Principles of Nano-Optics*. Cambridge University Press, 2012.